M. A. Vitrani
Laboratoire de Robotique de Paris (LRP), 18,
Route du Panorama-BP 61,
92265 Fontenay-aux-Roses Cedex,
France

J. Nikitczuk
Department of Mechanical and Industrial
Engineering,
Northeastern University,
375 Snell Engineering Center,
360 Huntington Avenue,
Boston, MA 02115

G. Morel
Laboratoire de Robotique de Paris (LRP), 18,
Route du Panorama-BP 61,
92265 Fontenay-aux-Roses Cedex,
France
e-mail: morel@robot.jussieu.fr

C. Mavroidis[1]
e-mail: mavro@coe.neu.edu

B. Weinberg

Department of Mechanical and Industrial
Engineering,
Northeastern University,
375 Snell Engineering Center,
360 Huntington Avenue,
Boston, MA 02115

Torque Control of Electrorheological Fluidic Resistive Actuators for Haptic Vehicular Instrument Controls

Force-feedback mechanisms have been designed to simplify and enhance the human-vehicle interface. The increase in secondary controls within vehicle cockpits has created a desire for a simpler, more efficient human-vehicle interface. By consolidating various controls into a single, haptic feedback control device, information can be transmitted to the operator, without requiring the driver's visual attention. In this paper, the experimental closed loop torque control of electro-rheological fluids (ERF) based resistive actuators for haptic applications is performed. ERFs are liquids that respond mechanically to electric fields by changing their properties, such as viscosity and shear stress electroactively. Using the electrically controlled rheological properties of ERFs, we developed resistive-actuators for haptic devices that can resist human operator forces in a controlled and tunable fashion. In this study, the ERF resistive-actuator analytical model is derived and experimentally verified and accurate closed loop torque control is experimentally achieved using a non-linear proportional integral controller with a feedforward loop. [DOI: 10.1115/1.2192822]

1 Introduction

In recent years, the proliferation of secondary controls within vehicles has created a desire to develop mechanisms to simplify and enhance the human-vehicle interface. A better interface technology is sought to facilitate driver access to a growing array of vehicle secondary functions, such as advanced audio features, climate controls, telecommunications and navigation. Electro-rheological fluids (ERF) based force-feedback mechanisms have been developed to address these issues. ERFs are liquids that respond mechanically to electrical stimulation by changing their viscosity electroactively. Using the electrically controlled rheological properties of ERFs, haptic devices have been developed that can resist human operator forces in a controlled and tunable fashion.

Instrument controls have haptic properties to maximize the ease of use for vehicle occupants. A single force-feedback knob can emulate the feel of conventional control knobs (detents, limit stops, friction) and can produce new effects as well such as vibration, scrolling, and free-spin, all instantaneously reconfigurable under computer control. Such a haptic knob can simulate the functions of all instrument controls that it replaces and thus reduced to one device, the control of the dashboard provides the driver with instant access to all functions, quickly and ergonomically. Figure 1 illustrates the concept of a multi-function haptic knob for vehicular instrument controls.

Several rotary force-feedback control knobs have been proposed for use in vehicular control that use a motor and a microprocessor controller to achieve the desired effect [1–4]. However, the magnitude of the torque available from these devices is limited by the size of the motor and its power consumption, both of which must be limited for practical use in a vehicle. To address some of these issues, a haptic knob has been developed that incorporates a brake to provide high torque capability in a small volume with low power consumption [5]. A magneto-rheological fluid (MRF)-based brake [6] improves the performance characteristics, however a large magnetic circuit is needed to generate a sufficient magnetic field. By using electro-rheological fluids it is possible to overcome the remaining limitations to further enhance the development of haptic interfaces for vehicular control. Specifically, it is possible to decrease the size, weight, and power consumption while increasing torque/force capability and device degrees-of-freedom. By using an electro-rheological fluid (ERF) it is possible to develop compact haptic devices since the ERF and its electrodes could be incorporated within the structure of the device, thus saving a lot of space. The compactness property satisfies the strict geometric constraints provided by the car manufacturers about the size of the haptic interfaces. ERFs are low power materials and hence the ERF based haptic interfaces are low power devices which is a property very much desired by the car manufacturers. Furthermore, the ERF device's small overall size allows

[1]To whom correspond address should be addressed.

Contributed by the Dynamic Systems Division of ASME for publication in the JOURNAL OF DYNAMIC SYSTEMS, MEASUREMENT, AND CONTROL. Manuscript received January 25, 2004; final manuscript received June 9, 2005. Assoc. Editor: Hemant M. Sardar.

Fig. 1 Artist's view of a multi-function haptic knob for vehicular instrument control

the addition of degrees of freedom without adding too much space. This characteristic is very important since it will increase the "dexterity" of the force-feedback device by being able to program a larger number of functions.

During the last 50 years, it has been known that there are liquids that respond mechanically to electrical stimulation. These liquids change their viscosity electroactively and they have attracted a great deal of interest of engineers and scientists. These electro-rheological fluids (ERF) exhibit a rapid, reversible, and tunable transition from a fluid state to a solid-like state upon the application of an external electric field [7]. Some of the advantages of ERFs are their high yield stress, low current density, and fast response (less than 1 ms). ERFs can apply very high electrically controlled resistive forces while their size (weight and geometric parameters) can be very small. ERFs are also not abrasive, non-toxic, and non-polluting (meet health and safety regulations). ERFs can be combined with other actuator types such as electromagnetic, pneumatic, or electrochemical actuators so that novel, hybrid actuators are produced with high power density and low energy requirements [8]. The electrically controlled rheological properties of ERFs can be beneficial to a wide range of technologies requiring damping or resistive force generation. Examples of such applications are active vibration suppression and motion control. Several commercial applications have been explored, mostly in the automotive industry for ERF-based engine mounts, shock absorbers, clutches, and seat dampers. Other applications include variable-resistance exercise equipment, earthquake-resistant tall structures, and positioning devices [7].

During the last ten years, some researchers proposed the use of ERFs in an effort to improve the performance of haptic interfaces. There are many properties of ERFs that can greatly improve the design of haptic devices. Their high yield stress, combined with their small sizes, can result in miniature haptic devices that can easily fit inside the human palm without creating any obstructions to human motion. ERFs do not require any transmission elements to produce high forces, so direct drive systems can be produced with less weight and inertia. Finally, ERFs respond almost instantly, in milliseconds, which can permit very high bandwidth control important for mirroring fast motions. The use of ERFs for tactile sensing in robotic fingers was proposed in Ref. [9]. Based on that work, several workers proposed the use of ERFs in tactile arrays used to interact with virtual environments [10] and also as assistive devices for the blind to read the Braille system as proposed in Ref. [11]. Continuing this work, a 5×5 ERF tactile array was developed and tested experimentally [12]. An ERF-based planar force-feedback manipulator system that interacts with a virtual environment was described in Ref. [13]. This system is actuated by low-inertia motors equipped with an ER clutch. An ERF-based force-feedback joystick has been developed in Ref. [14]. The joystick consists of a ball and socket joint where ERF has been placed in the space between the ball and the socket. The operator feels a resistive force to his/her motion resulting from the controlled viscosity of the ERF.

While a lot of research has been performed on the design, modeling, and testing of ERF based resistive devices, little work has been performed on their closed loop control. Most of the literature in this area studied the position control [15] while very little work has been performed on the force/torque control of these devices. ERF devices are generally used with position control as dampers to avoid vibration [16], such as in vehicle suspensions [17] or for developing anti-seismic buildings [18]. Position control has also been applied in ERF devices such as valves [19]. Force control applications of ERFs have been studied in Ref. [20] where the tip of a robotic finger was equipped with an ERF actuated component that acts as an actively controlled damper. This allows optimal absorption of the impulse forces at the contact transitions, while the explicit force control of the finger is left to a conventional dc motor. On the contrary, in the present paper, an ERF-based resistive actuator is used for the explicit force control of the haptic knob, without the need of an additional actuator.

Our group has developed and studied several ERF based haptic systems [21,22]. The joints of these systems are powered by specially designed ERF based resistive actuators. In our work we use the term "resistive actuator" to denote the fact that these ERF actuating elements are only capable of generating reprogrammable, computer controllable, and time varying resistive forces or torques to any externally applied load on the haptic interface. Recently we developed prototypes of rotary ERF based resistive actuating elements for haptic knobs for vehicular instrument controls [23]. The present paper focuses on the torque control of this device and its application for the creation of haptic illusions. Section 2 briefly recalls the fundamentals of ERF modelling, while Sec. 3 shows how the fluid model can be used to derive the resistive actuator model. As many parameters of the model were not precisely known, an experimental identification of the resistive actuator behavior had to be performed and is summarized in Sec. 4. The experimentally identified model was then used in a torque control loop whose design is detailed in Sec. 5. This is the first time that closed loop torque control of ERF devices is achieved using a non-linear proportional integral controller. Finally, the programming of haptic illusions with the closed-loop torque controlled ERF resistive actuator is demonstrated. Indeed, conventional control schemes, mainly based on stiffness selection, could not be used in such an ERF based resistive actuator, because it cannot behave as a spring. Rather, an original method, presented in Sec. 6, was developed. With this approach, haptic illusions are created by computing the desired torque fed to the torque controller, not only from positions, as usual, but also from the measured torque, in order to analyze what the user is doing and to react appropriately.

2 Fundamentals of Electro-Rheological Fluids

ERFs are suspensions of polarizable particles in a viscous nonconducting oil with particle-fluid dielectric mismatch. Typical suspended particles in an ERF are approximately spherical and $1-100$ μm diameter long, while the suspending fluids are nonconducting solvents [24–27]. When an uncharged particle is placed in an electric field, it develops an induced dipole if the surrounding medium has a different dielectric constant due to the differing polarizability of the two materials. This dipole is further enhanced by the presence of other particles since they intensify the local electric field experienced by any one particle. Particle polarization changes their organization in the fluid and causes changes in fluid rheological properties. The changes in the suspension microstructure increase the effective viscosity of a sheared ERF, which is known as the Winslow effect [28]. The effective viscosity of the ERF suspension can be 100,000 times greater for electric field strengths of about 1 kV/mm perpendicular to the direction of flow. Since the discovery of the electrorheological

phenomenon, a lot of research has been performed to develop a behavior model of ERF [29]. The well-known one is the Bingham model.

Modeling the behavior of an ERF is generally performed by using a known conventional fluid (or even solid-plastic) model, thus defining the basic structure of the model, and then characterizing how the model parameters are affected by the application of an electric field, or by the variation of some internal state variables, such as temperature or the type of flow [30]. Under zero field conditions, ERFs are generally characterized by a simple Newtonian viscosity. When subjected to high electric fields, ERFs develop a yield stress and their shear stress τ is fairly well modeled as a Bingham plastic:

$$\tau = \mu\dot{\gamma} + \tau_{y,d} \tag{1}$$

where μ is the plastic viscosity, $\dot{\gamma}$ is the shear rate and $\tau_{y,d}$ is the Bingham or dynamic yield stress.

One can conclude by extrapolation to zero shear rate that the stress must exceed this dynamic yield stress in order for the material to flow, similarly to a dry Coulomb friction model. In fact, the minimum stress required to cause the ERF to flow is not necessarily the dynamic yield stress but rather the static yield stress $\tau_{y,s} > \tau_{y,d}$. Using the friction analogy, this can be understood as the well-known Stribeck effect. More precisely, there are three yield stresses characterizing the behavior of an ERF [31]. The first is the elastic-limit yield stress τ_e, which is used, in solid mechanics. Upon complete removal of the stress exceeding τ_e, the material never fully recovers and suffers a permanent strain γ_e, which is the transition between elastic and plastic deformation. The elastic-limit yield stress is not the limit of linear behavior but rather the limit of reversibility for the material. Loss of linear behavior generally occurs before the elastic limit. The static yield stress τ_s is the minimum stress necessary for the unbounded strain or the deformation of the material. Finally, the plateau stress for large strains is the dynamic yield stress τ_d.

The Bingham plastic model has been widely used to predict the post-yield behavior of ERF, i.e., the behavior of the ERF when flowing. However, if the fluid experiences shear thinning or thickening, the Bingham plastic model may not be an accurate predictor of the behavior since the post-yield plastic viscosity is assumed to be constant. When shear thinning or thickening effect is more pronounced, the post-yield behavior becomes non-linear. In order to accurately model this non-linear post-yield (or flowing) behavior, another generic fluid model should be used that is called the Herschel-Bulkley model [32]:

$$\tau = \tau_{y,d} + \mathrm{k}\dot{\gamma}^n \tag{2}$$

This fluid model is a generalized model for visco-plastic flow with yield stress. It can be reduced to the Bingham plastic model (namely, $n=1$) in the case where post-yield shear thinning or thickening are minimal. In regard to the Bingham model described by Eq. (1), the applied electric field E affects the dynamic yield stress, with a quadratic relationship. This yields

$$\tau_{y,d} = \alpha E^2 \tag{3}$$

The ERF used in this project is the LID 3354S manufactured by Smart Technology Ltd. [33]. It is made up of 35% by volume of polymer particles in silicone/fluorolube base oil. According to the provider, the field dependencies for this particular fluid are

$$\tau_{y,s} = C_s(E - E_{\mathrm{ref}})$$

$$\tau_{y,d} = C_d E^2$$

$$\mu = \mu_0 - C_v E^2 \tag{4}$$

where μ_0 is the zero field viscosity, C_s, C_d, C_v, and E_{ref} are constants whose approximate values are supplied by the manufacturer. Obviously, the formula for the static yield stress is only valid for fields greater than E_{ref}. In this work, it is assumed that the torque controller will be used to finely control the resistive torque of a device that is moved by an operator (or by an auxiliary motor) and therefore only the dynamic mode is considered.

A very important phenomenon in the operation of ERFs that can cause serious controls problems is the effect of "arcing." It can be observed that after a certain voltage, usually very high, the ERF will present arcing between its electrodes which will result in loss of the control of the ERF and its properties for a very small amount of time. In the case of ERF resistive actuators that are studied in this paper, arcing can be seen as a saturation of the actuator, which means that there is a maximum limit of voltage that can be applied between the actuator electrodes. Above this maximum/saturation voltage limit the actuator will not be able to function. Arcing releases the stored energy in the fluid (de-energizes the electric field) causing the activated ERF to return to its liquid state. A high performance high-voltage power supply will re-energize the fluid quickly, but in practice, there will be several hundred milliseconds with no control over the fluid and its resistive properties. Current leakage through the ERF during arcing results in heat build up and negatively affects the properties of the ER fluid, resulting in increased power consumption and reduced fluid life. At the design level, there are several details that can reduce the chances of arcing. One should eliminate all sharp edges from the electrodes of the ERF device since local charge concentrations form at these edges; this is similar to the lightning rod effect during a thunderstorm. It is also important to make sure that the electrodes are evenly spaced apart and are parallel. Field strength is directly proportional to gap size, so any misalignment, wobble, or electrodes that are improperly spaced will increase the chances of arcing. By following these design guidelines it is possible to increase considerably the maximum voltage (saturation limit) that can be applied to an ERF resistive actuator.

3 The FP Resistive Actuator and its Model

A haptic feedback joystick and knob have been developed by our team to address the desire for simplifying and enhancing the human-vehicle interface [23]. They are used in this paper as the test-bed to perform closed loop torque control experiments and initial haptic knob tests. The studied ERF resistive actuator consists of multiple parallel rotating electrode plates. This allows for enhancing the resistive torque output capability by increasing the activated area of the fluid while maintaining a compact volume. Figure 2 shows the components and assembly of the flat-plate or FP resistive actuator. Two shafts are designed and situated in a concentric orientation with one shaft fixed to the housing of the device and the second able to rotate against the fixed shaft (Fig. 2(*a*)). Circular copper plates connected to the shafts (Fig. 2(*b*)) serve as the positive and negative electrodes that generate the electric field to actuate the ERF that sits inside the gap. These separate shaft-plate assemblies are fit together (Fig. 2(*c*)) to form the multiple-plate, and then inserted into a housing that is filled with ERF (Fig. 2(*d*)). The shaft-plate assemblies are mounted to an enclosure which contains bearings and a seal to prevent leakage of the ERF or of its vapors. Preventing vaporization of the fluid virtually eliminates the effect of suspension settling after long periods of time. Considerable effort was made to reduce the friction caused by the seal. Figure 3 shows a cut-away view of the assembled multiple flat-plate ERF resistive actuator and a picture of the experimental prototype. The plastic parts of the prototype were built using rapid prototyping methods to allow for the quick creation of complicated shapes that would not have been possible with machine shop methods. The copper plates were machined, however, using more traditional methods. Table 1 shows the values of the important parameters of the FP resistive actuator prototype.

Figure 4 defines important geometric parameters that are used in order to develop a model for the FP resistive actuator. Providing a model of the device from the fluid model supposes to map the shear stress into the output torque and the shear rate into the

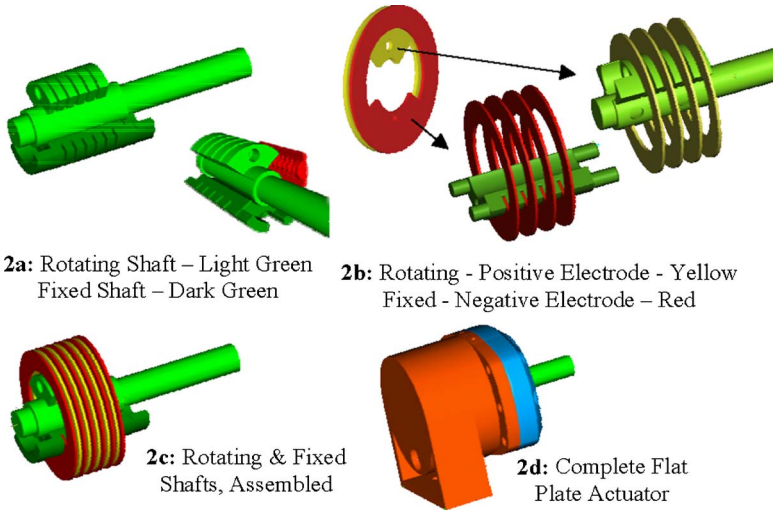

Fig. 2 Components and assembly steps for the flat plate resistive actuator

output velocity. To do so, we assume that the shear stress is constant along a line parallel to the axis, between the electrodes. Due to the symmetry of the system, the shear stress is supposed to depend only on the radius r, not on the angle θ. The elementary resistive torque between a pair of electrodes is then

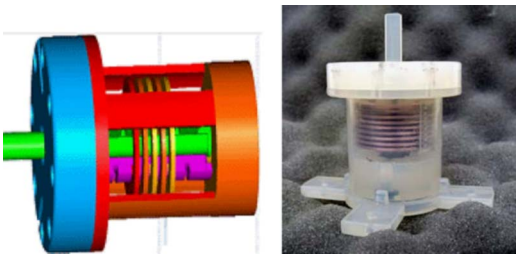

Fig. 3 Assembled multiple flat-plate ERF resistive actuator: CAD drawing (left) and experimental prototype (right)

Table 1 Values of flat-plate (FP) ERF resistive actuator important parameters

Outer radius	14.7 mm
Length	32.5 mm
Gap width	0.5 mm
Dynamic torque at 2 kV	188.5 mN m
Dynamic torque at 4 kV	753.4 mN m
Range of motion	120°
Number of plates	15

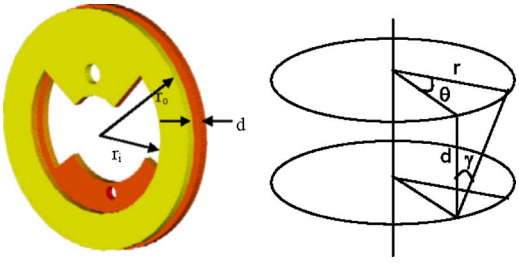

Fig. 4 FP resistive actuator model geometric parameters

$$T_{\text{ele}} = \int_{r_i}^{r_0} r\tau(r)dA \tag{5}$$

where $dA = 2\pi r dr$ and $\tau(r)$ is the shear stress at a radius r from the axis.

Since N rotating plates are mounted in between $N+1$ fixed plates, there are $2N$ gaps filled with ERF, producing a total resistive torque given by

$$T_a = 2NT_{\text{ele}} = 4\pi N \int_{r_i}^{r_0} r^2\tau(r)dr \tag{6}$$

Furthermore, for a displacement $\delta\theta$ of the device, the (angular) shear deformation of a fluid element $\delta\gamma$ (see Fig. 5) at a radius r is

$$\delta\gamma = \frac{r}{d}\delta\theta \tag{7}$$

The relationship from the angular velocity to the shear rate is then

$$\dot{\gamma} = \frac{r}{d}\dot{\theta} \tag{8}$$

Thus, combining Eqs. (1), (4), and (8), one gets

$$\tau(r) = C_d E^2 + (\mu_0 - C_v E^2)\frac{r}{d}\dot{\theta} \tag{9}$$

Combining Eq. (9) with Eq. (6), we obtain

$$T_a = 4\pi N \int_{r_i}^{r_0} r^2\left(C_d E^2 + (\mu_0 - C_v E^2)\frac{r}{d}\dot{\theta}\right)dr \tag{10}$$

which finally leads to:

$$T_a = 4\pi N\left[C_d\frac{r_0^3 - r_i^3}{3} - C_v\frac{r_0^4 - r_i^4}{4d}\dot{\theta}\right]E^2 + \pi N(r_0^4 - r_i^4)\frac{\mu_0}{d}\dot{\theta} \tag{11}$$

Furthermore, in order to produce the electric field, a positive voltage V_p is applied to the fixed plates, while the rotating plates, which geometrically alternate with the fixed ones, are grounded. The field is then the same in all the inter-plate gaps, and is simply given by

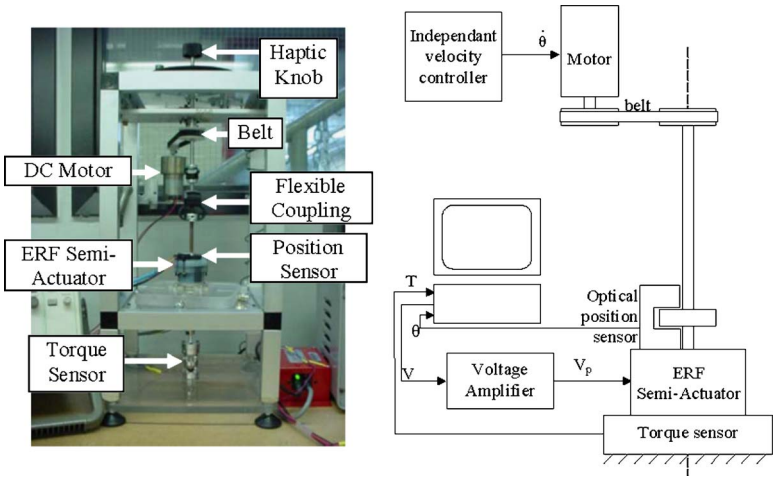

Fig. 5 Experimental setup of a haptic knob

$$E = \frac{V_p}{d} \tag{12}$$

The final model of the actuator can then be written as

$$T_a = (\alpha_0 - \alpha_1 \dot{\theta}) V_p^2 + \alpha_2 \dot{\theta} \tag{13}$$

where α_i, $i \in [1, \ldots, 3]$ are constant positive scalars given by

$$\alpha_1 = \frac{\pi 4 N C_d (r_0^3 - r_i^3)}{3d^2}$$

$$\alpha_1 = \frac{\pi N C_v (r_0^4 - r_i^4)}{d^3}$$

$$\alpha_2 = \pi N (r_0^4 - r_i^4) \frac{\mu_0}{d} \tag{14}$$

The device also exhibits friction that does not arise from the fluid itself, but from other mechanical parts, such as sealing. This additional friction torque T_f is modeled as the sum of a dry friction term T_{fd} and a viscous friction coefficient β_f. The final resulting torque is then

$$T = T_a + T_f = (\alpha_0 - \alpha_1 \dot{\theta}) V_p^2 + \alpha_2 \dot{\theta} + T_{\text{fd}} \operatorname{sign}(\dot{\theta}) + \beta_f \dot{\theta} \tag{15}$$

Finally, it was experimentally observed that the system experiences a slightly hysteretic behavior, which is not accounted for in this model. Modeling of hysteresis could be performed by the use of a complex mathematical description such as Preisach modeling. However, the off line identification of such a model involves a large number of parameters. Moreover, the use of such a model for control purposes requires robust on line matching of the model parameter values, and it is still an open research issue that is beyond the scope of this paper. As a consequence, the static behavior given by Eq. (15) was kept as the nominal model of the resistive actuator. To compensate for the small error that is generated by neglecting the hysteretic behavior, a proportional-integral (PI) term was used in the controller (see Sec. 5), thus canceling the steady state error in spite of the modeling uncertainties.

In the model of Eq. (15), no transient dynamics have been included. Namely, the yield torque, at a given velocity, is supposed to settle instantaneously when applying a voltage. In fact, both literature and the fluid provider report time response as short as 1 ms, which can be considered as an instantaneous response, since the system will be digitally controlled with a 5 ms sampling period. In terms of dynamics, the dominant pole of the system is the pole of the amplifying electronics, which transforms the low voltage output V generated by the control computer into the high voltage V_p applied to the electrodes:

$$V_p = \frac{G}{1 + \tau_e s} V \tag{16}$$

where the static gain $G = 1000$ is given by the electronics provider while the time constant τ_e was experimentally identified: $\tau_e = 25$ ms.

In summary, from the command output V to the torque T, the resistive actuator model can be viewed as a cascade between a linear transient dynamics term described by Eq. (16) and a nonlinear static component, with a secondary input $\dot{\theta}$, described by Eq. (15).

4 Experimental Parameter Identification

To test the performance of the FP resistive actuator prototype, as well as to experimentally validate its theoretical model and to perform closed loop torque control experiments, an experimental setup shown in Fig. 5 was developed. The FP resistive actuator shaft is attached to a flexible coupling to ensure proper alignment. The other side of the flexible coupling is connected to a dc motor through a belt with a pulley wheel. This motor is velocity controlled by an independent system. The FP resistive actuator will controllably resist the externally applied torques. An optical encoder attached to the shaft is used to measure the angular displacement. A torque sensor is attached at the base of the FP actuator to measure its resistive torque output. In this experimental setup, two parameters can be changed by the user: the velocity of the motor and the voltage applied to the fluid.

A PC augmented with a US Digital® PC7166™ PC to incremental encoder interface card and a Datel® PC-412C™ Analog I/O board was used in the open and closed loop experiments. The PC collects the sensor measurements, that is the torque T through the data acquisition board and the rotational angle θ from the encoder interface card, performs the feedback control calculation and then it sends out the voltage V to the FP resistive actuator, through the D/A converter and laboratory built amplifiers.

Our objective in this section is to verify the ability of Eq. (15) to describe the static post-yield behavior of the resistive actuator and experimentally identify the model parameters. First, experiments are performed with a constant speed of the dc motor that provides the input torque to the FP resistive actuator. Then, the same experiments are performed with different constant speeds. In order to avoid the excitation of internal hysteretic cycles, that

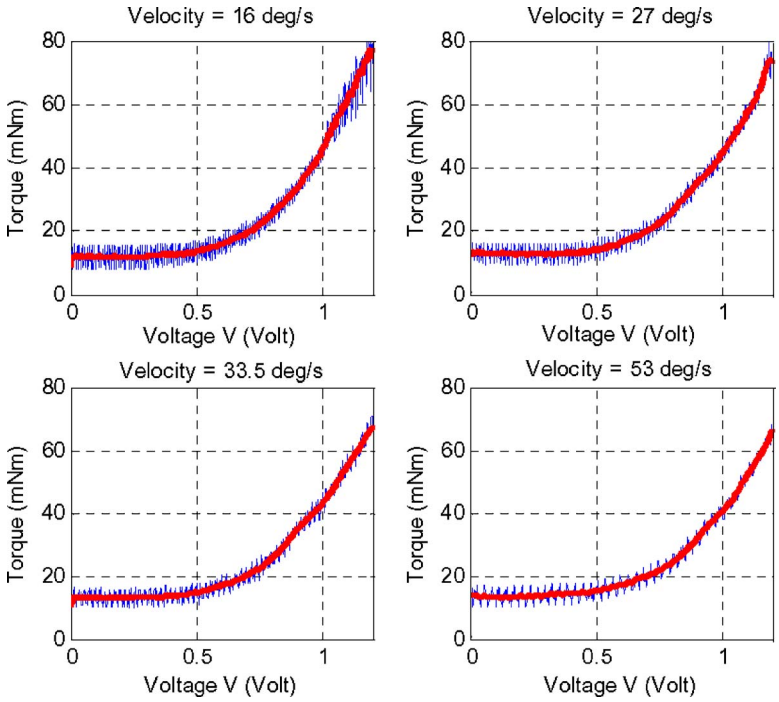

Fig. 6 Reactive torque response for different velocities

would corrupt the parametric identification, a careful repetitive procedure is used as follows for each experiment with constant speed:

(a) The device is initially placed at $\theta=0°$.
(b) The motor starts and obtains a constant velocity, and a ramp voltage is applied to the ERF. It is verified that the ramp slope is slow enough compared to the expected resistive actuator dominant dynamics. As a result, a quasi-static behavior can be assumed. When applying the ramp voltage, the resistive torque is measured.
(c) When this experiment is over, the resistive actuator is put back in the initial position with a null electric field.
(d) It is then verified that, redoing the experiment from step a), the torque response is repeatable.

On Fig. 6, lines in blue show typical results of the torque-voltage relationship for four different velocities of the dc motor.

From Fig. 6 it can be verified that the response shape agrees with Eq. (15). It can be noticed that, below a certain voltage limit V_{lim}, which depends on the velocity, the ERF seems reactionless. Note that this is in accordance with Eq. (4), which describes the static preyield behavior, although what is measured here is the dynamic mode. To account for this experimentally emphasized phenomenon, and taking into account that the experiments were performed with constant speed, Eq. (15) can be written as

$$T=\begin{cases} T_0 & \text{if} \quad V<V_{\text{lim}} \\ T_0+k & (V-V_{\text{lim}})^2 \quad \text{otherwise} \end{cases} \tag{17}$$

where T_0 is the minimal torque measured with a zero voltage, V_{lim} is the voltage under which nothing happens.

The three parameters of a constant speed experiment, namely T_0, k, and V_{lim} are then computed in order to obtain a least square best fit. In Fig. 6, the red lines show the best fits of this model for the different velocities. The identified parameters T_0, k, and V_{lim} are different for each experiment, which denotes their dependency on velocity. The identified parameters for several velocities are reported in Table 2.

In turn, a best fit is used to express the velocity dependency of these three parameters. It is found that the three parameters are linear functions of the velocity. Namely:

$$T=T_0+k(V-V_{\text{lim}})^2 \quad \text{with} \begin{cases} T_0=17.25\ \text{sign}(\dot\theta)+0.0625\dot\theta \\ k=123\ \text{sign}(\dot\theta)+0.5\dot\theta \\ V_{\text{lim}}=\begin{cases} 0.3+7\,.\,10^{-4}\dot\theta & \text{if } \dot\theta<0 \\ 0.45-7\,.\,10^{-4}\dot\theta & \text{if } \dot\theta>0 \end{cases} \end{cases} \tag{18}$$

where V is the computer output voltage expressed in volts (which is also the ERF applied voltage expressed in kV) and the torques are expressed in mNm. Note that the velocity dependency confirms, in part, the theoretical model. For example, the coefficient k decreases with the velocity, as the expected effect of the positive scalar α_1. Also, the zero field torque T_0 is the sum of a dry friction term (17.25 mNm) and a viscous term, as expected.

Figure 7 shows the 3D plot mapping of the FP resistive actuator resistive torque output as a function of the applied voltage (V) and of the dc motor velocity ($\dot\theta$) using the experimental identified model. Experimental results have been superimposed with different colors for different velocities. Experimental curves fit well the

Table 2 Experimental value of the parameters

Velocity (deg/s)	T_0 (mNm)	K	V_{lim} (V)
53	20.7	78	0.41
33.5	20	100	0.45
27	19.7	110	0.45
16	18.3	120	0.45
−16	−18.4	−105	0.3
−26	−18.9	−97	0.3
−32.5	−18.8	−87	0.3
−50	−20	−65	0.2

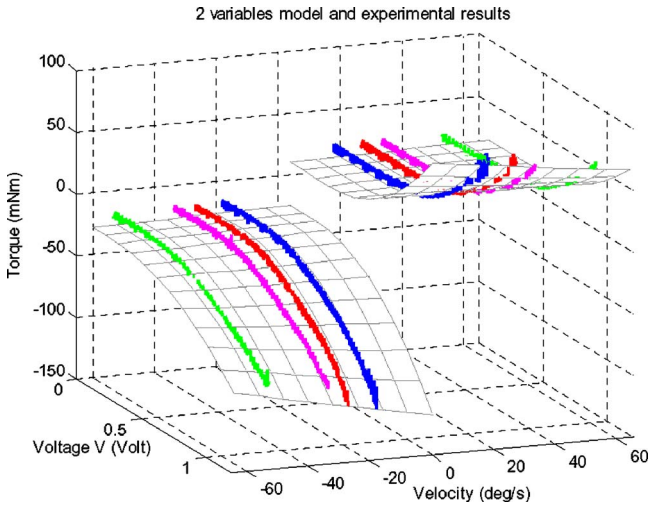

Fig. 7 FP resistive actuator resistive torque as a function of input voltage and rotational speed

model's 3D plot mapping, which illustrate the accuracy of the identified model. Again, recall that this accuracy is obtained thanks to a careful procedure that was aimed at preventing hysteretic internal cycles from occurring. Should a hysteretic cycle occur, the model would not be as precise as depicted in Fig. 7.

When controlling the device, one will need to use the resistive actuator model identified with Eq. (18) to convert desired torques to input voltages in the ERF. To do so Eq. (18) needs to be inverted so that it calculates the voltage V as a function of the command torque $\tilde{T}$ and of the actuator velocity $\dot{\theta}$:

$$V(\tilde{T},\dot{\theta}) = V_{\lim}(\dot{\theta}) + \sqrt{\frac{\tilde{T} - T_0(\dot{\theta})}{k(\dot{\theta})}} \tag{19}$$

To be able to use Eq. (19) the following constraint needs to be satisfied:

$$T(V,\dot{\theta}) - T_0(\dot{\theta}) \geqslant 0 \tag{20}$$

Inequality (20) means that the desired resistive torque that the resistive actuator should produce must be larger than $T_0(\dot{\theta})$, i.e., the minimal torque measured with a zero voltage, which is the sum of a dry friction term and a viscous term depending on the velocity. In cases where the desired torque is such that inequality (20) is not satisfied, i.e., when the applied voltages are between zero and $V_{\lim}$, a linear interpolation is used to calculate the applied voltage:

$$V(\tilde{T},\dot{\theta}) = V_{\lim}(\dot{\theta})\frac{\tilde{T}}{T_0(\dot{\theta})} \tag{21}$$

Equation (21) does not correspond to any physical model, but it is used to provide inverse model continuity when the voltages are lower than $V_{\lim}$. In order to validate this inverse model, a set of open loop experiments were performed. During these experiments, the motor speed was set to a constant value, then a ramp desired torque was provided, and the inverse model was used to compute the command Voltage V corresponding to this desired torque, from Eqs. (19) and (21). The resistive torque of the FP resistive actuator was measured using the torque sensor and compared to the desired one. Some representative results from these experiments are shown in Fig. 8, emphasizing a reasonable precision of the model.

5 Closed Loop Torque Control

Two different closed loop controllers were considered: (a) a simple, model free, linear proportional-integral (PI) controller and (b) a non-linear, model based, PI controller with a feed-forward term. Figure 9 shows the block diagram of the linear PI controller without using the identified model.

In order to tune the proportional K_p and integral K_i gains, the dominant pole of the voltage amplifier was canceled by choosing K_p/K_i=25 ms, while K_p was manually tuned up in order to obtain a well damped response. The gains were tuned for a desired torque stepping from 25–30 mNm. The finally tuned gains are K_p=0.015 V/mNm and K_i=0.6 V/s mNm. Figure 10 shows the

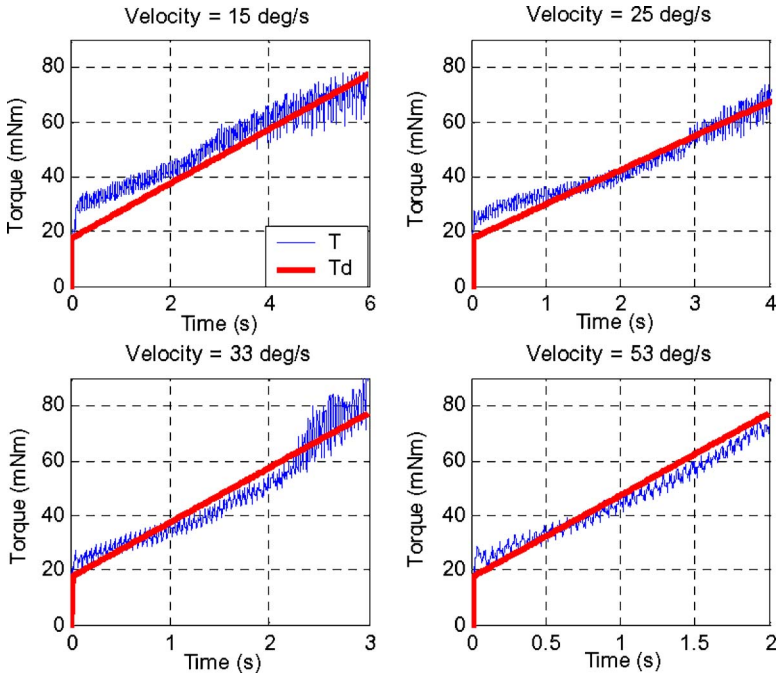

Fig. 8 Experimental verification of the inverse model

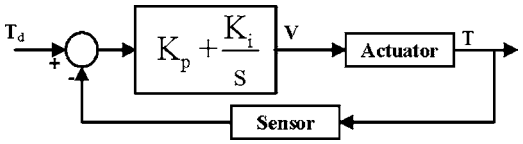

Fig. 9 Linear PI controller

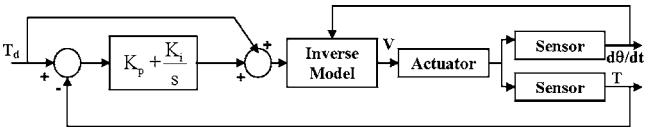

Fig. 11 Non-linear PI controller with feed-forward term

results from two different step inputs, one on the left with a low and another on the right with a high desired torque input.

The graphs on the left of Fig. 10 show a well-damped response for a desired torque stepping from 25 to 30 mNm. The graphs on the right, which are obtained with the same controller, for a desired torque stepping from 45 to 50 mNm, indicate a large overshoot. The fact that the response is well damped for low torques while the system exhibits a high overshoot if the desired torque is large, can be explained by the non-linearity between the output torque and the input voltage. For low torques, a small change in the voltage leads to a small change in the reactive torque. The same small change in the voltage leads to a large change in the resistive torque output for high torques. This can be seen in Fig. 10 where 0.35 V are needed to increase the torque by 5 mNm in low torques, and only 0.15 V for a high torque. This illustrates the well-known fact that a linear controller, when used with a nonlinear plant, exhibits a closed loop response that depends on the state of the system. The linearizing effect of the closed loop is only partial. That is why a nonlinear controller was investigated and is presented in the rest of this section.

Figure 11 shows the block diagram of a non-linear, model based PI controller with a feed-forward term. A control error is fed into a PI controller. The command torque is the sum of the output from the PI controller and a desired torque feedforward term. The latter is used so that the PI compensator works with small values of inputs and outputs. The command torque is converted to a control voltage using the non-linear Equation (19). The PI controller is manually tuned in order to achieve a fast and damped response. The final gains are K_p=0.6, K_i=100 s^{-1}. Some representative results from the experiments with this controller are shown in Fig. 12. It can be clearly seen that the response is fast (settling time is approximately 70 ms) and well damped. The response is reproducible for any value of the desired torque input, which indicates a successful linearization. Extensive experiments have demonstrated a strong robustness of the controller to variations of experimental conditions, such as the magnitude and sign of velocity. The closed loop dynamics are rather constant, even when the resistive actuator is cycled arbitrarily, i.e., when its hysteretic behavior is excited.

6 Creating a Haptic Sensation With the FP Resistive Actuator

A major difficulty in creating a haptic sensation with ERF-based devices is that they are semi-active systems. Because an FP resistive actuator is not a fully active device, a number of classical illusions in haptics cannot be realized as easily as when using fully active devices.

For example, assume that it is desired to create an artificial limit to a knob rotation. In conventional control of haptic devices, this is achieved by creating a virtual spring with controllable stiffness (see Fig. 13(*a*)). With a fully actuated device, the haptic function consists of generating a desired torque to feed the inner torque loop, using sole position measurement as an input (Fig. 13(*b*)).

More precisely, in the case of the spring function, using the notations of Fig. 13, the haptic function would be:

$$\text{if } \theta < \theta_0 \quad \text{then } T_d = 0 \quad \text{else } T_d = f(\theta) = k(\theta_0 - \theta)$$

It can be observed that in this case, the desired torque can be achieved independently of what the operator does. For example, assume that the operator turns the knob up to a certain angle θ, by exerting a torque $k(\theta_0 - \theta)$. At the equilibrium, the knob exerts a torque equal and of opposite sign to the operator. If the operator releases the handle, the actuator will still exert the same torque (since it is active), producing a knob angular acceleration, which

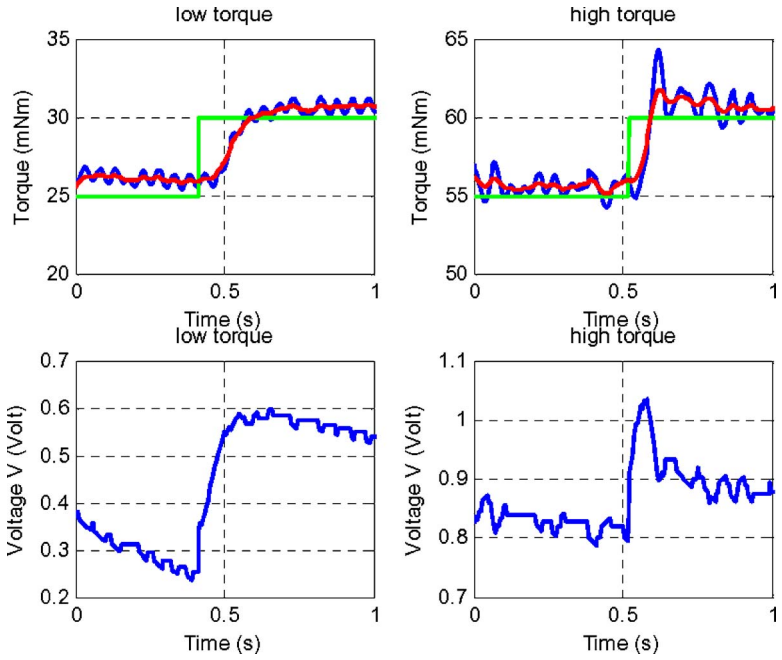

Fig. 10 Closed loop step response using a linear PI controller

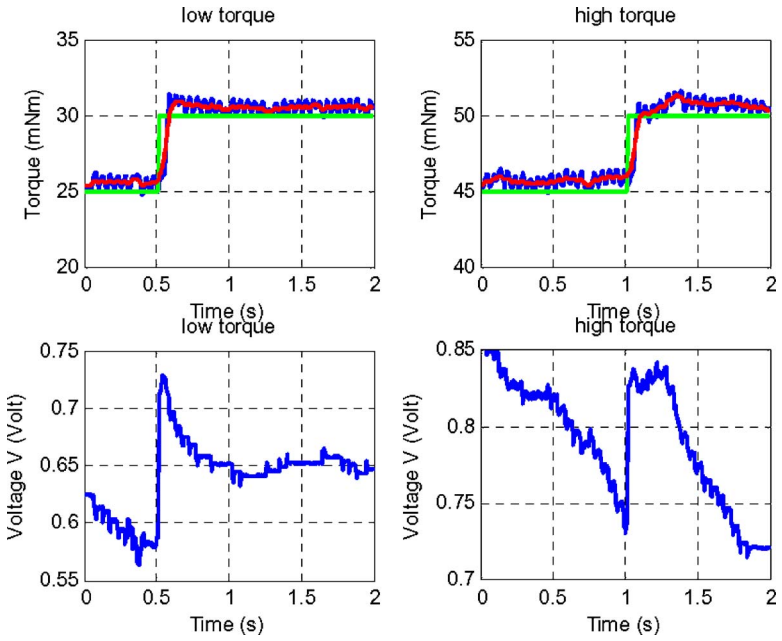

Fig. 12 Closed loop step response using a non-linear PI controller

will result in a back rotational motion of the knob until angle θ becomes smaller than the equilibrium position θ_0. Obviously, this cannot happen with a semi-active system. Indeed, if we'd apply the same haptic function $f(\theta)$ to a semi-active device, the system would exhibit the following behavior. When the operator starts turning, with the condition that the inner torque loop is fast and precise enough, the knob behavior is similar to that of a fully active device described above. When the operator releases the knob, the torque produced by the resistive actuator is zero, which means that the knob stays still. Furthermore, since $T_d=f(\theta)=k(\theta_0-\theta)$, there is a non-zero desired torque, resulting in a large control error. Due to the presence of an integrator within the torque loop, the actuator saturates to its maximal input voltage, corresponding to a resistive torque $T_{\max}$. If the operator wants the knob to get back to an angle $\theta<\theta_0$, he or she has to apply a negative torque. Since the desired torque does not change until θ changes, the operator will have to exert a torque larger (in absolute value) than $-T_{\max}$ to move the knob back.

For all these reasons stated above, to achieve a haptic sensation with an ERF based resistive actuator, it is required to implement a haptic function that uses as inputs not only the knob angle, but also the measurement of the torque applied by the operator. We consider here the haptic realization of a "click" function. Namely, what we want to provide is a minimal resistive torque over the knob angular range, except around a given position θ_0 where it has to click. Consider that the operator moves the knob with a positive velocity. Up to a certain angle $\theta_1<\theta_0$, the desired torque is zero. Then, when $\theta_1<\theta<\theta_0$, the system should resist increasingly, while, if $\theta>\theta_0$, the desired torque should instantaneously drop to zero in order to produce the feeling of a rapid release. Thus, for a positive motion, the following algorithm should be used:

$$
\begin{aligned}
&\text{if } \theta_1<\theta<\theta_0\\
&\quad \text{then if } T>0\\
&\qquad \text{then } T_d=T_{\max}\frac{\theta-\theta_1}{\theta_0-\theta_1}\\
&\qquad \text{else } T_d=0\\
&\text{else}\\
&\quad T_d=0
\end{aligned}
$$

Note that, even if $\theta_1<\theta<\theta_0$ the desired torque is set to zero when the applied torque is negative, which allows one to pull back the knob with no resistance if the user does not want to push over the click. In order to feel the click for both directions of rotation at the same position, it is required to implement a symmetric function for positions larger than θ_0 and negative torques, as illustrated in Fig. 14. Furthermore, in order to prevent the torque loop integrator from saturating when the operator releases the knob within the angular click domain, the torque controller output V is frozen whenever the applied torque is zero. Such a zero torque is actually

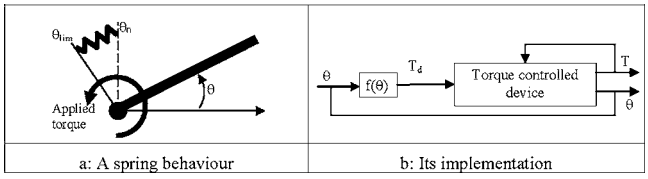

Fig. 13 Realizing a spring function with a fully actuated device

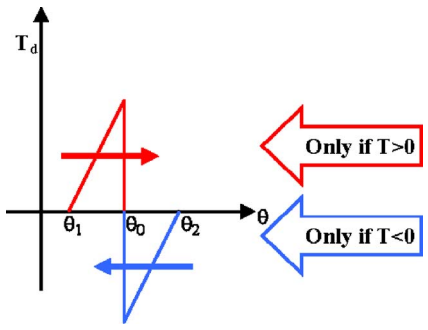

Fig. 14 The haptic function of a "click"

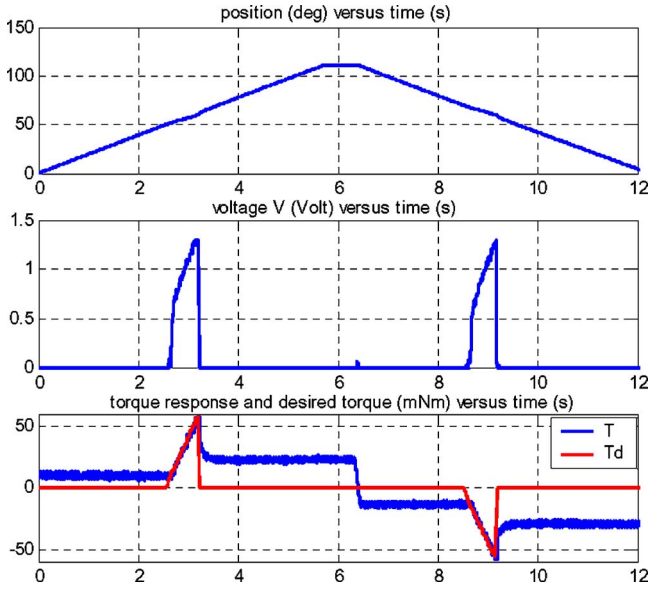

Fig. 15 Haptic sensation: Passing through a "click"

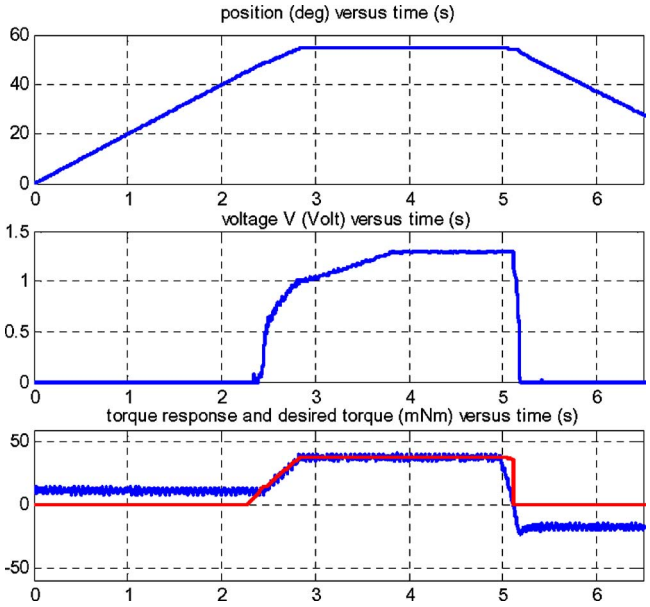

Fig. 16 Haptic sensation: Pushing, then pulling

detected within a dead zone of ±1.5 mN m, so as to deal with the measurement noise. Finally, the following algorithm is used to compute the desired torque:

$$
\begin{aligned}
&\text{if } \theta_1 < \theta < \theta_0 \\
&\quad \text{then if } T > 1.5 \\
&\qquad \text{then } T_d = T_{\max}\frac{\theta - \theta_1}{\theta_0 - \theta_1} \\
&\qquad \text{else if } T < -1.15 \\
&\qquad\quad \text{then } T_d = 0 \\
&\qquad\quad \text{else } V_{k+1} = V_k \\
&\text{else if } \theta_0 > \theta > \theta_2 \\
&\quad \text{then if } T < -1.5 \\
&\qquad \text{then } T_d = T_{\max}\frac{\theta_2 - \theta}{\theta_2 - \theta_0} \\
&\qquad \text{else if } T < -1.5 \\
&\qquad\quad \text{then } T_d = 0 \\
&\qquad\quad \text{else } V_{k+1} = V_k \\
&\text{else } T_d = 0
\end{aligned}
\tag{22}
$$

The parameters θ_0, θ_1, θ_2, and $T_{\max}$, can be tuned to produce different feelings. $T_{\max}$ represents the maximum resistance. Reducing the width $\theta_2 - \theta_1$ would produce a thinner clicker. However, this parameter has to be tuned considering also the dynamics of the torque loop and the maximum velocity of the knob. Indeed, if the operator rapidly turns the knob and if the programmed width is small, there is a risk that the reaction of the torque loop, which starts when $\theta > \theta_1$, is not complete when $\theta > \theta_0$. In this case, the desired torque comes back to zero and the click is not felt by the operator.

In addition to the inner nonlinear PI torque controller, Algorithm (22) has been implemented, with the following parameters: θ_0=60 deg, θ_1=55 deg, θ_2=65 deg and $T_{\max}$=60 mNm. In order to produce illustrative plots of the system behaviour, experiments were performed using the DC motor as an operator, thus producing a well controllable velocity.

In the first haptic experiment shown in Fig. 15, the click is passed one time in both directions. It can be observed that the desired torque is a ramp since the velocity is constant. The actual torque precisely follows the desired one, except when the desired torque is zero, which cannot be achieved by the resistive actuator due to the minimal amount of friction. This minimal amount is different before and after the click, which is due to the hysteretic effect. Interestingly, the click-release dynamics are very fast, as the actual torque drops to its minimal amount within less than 100 ms. In order to illustrate the ability of releasing the resistive torque when a back motion is desired prior to clicking, results from a second experiment are shown in Fig. 16. In this experiment, the dc motor is stopped when θ=57 deg, that is before clicking. The actual torque stays still until a reverse motion is commanded to the motor.

Then, the torque first decreases linearly due to the elasticity of the rod, and, when the torque becomes negative (the motor starts pulling), the desired torque drops to zero resulting in a minimal friction. This would not have been possible with a conventional haptic function.

7 Conclusions

The purpose of this research was to verify the possibility of using ERF based resistive actuators in haptic interfaces. To do this, an experimental method has been proposed to identify the behavior of the system. This model describes the resistive torque as a function of both the applied voltage and the velocity, and somehow confirms the general trends of the theoretical model. Next, torque control of an ERF based resistive actuator was investigated. The experimental inverse model was added to a PI controller in order to linearize the system. It has been shown that this non-linear PI controller with feedforward exhibits a precise and accurate response, compatible with a use in a haptic application. Then, the difficulty of using a resistive actuator as a haptic device has been emphasized. Semi-active or resistive actuators act as brakes. Thus, some classical haptic applications cannot be created and some others have to be re-designed in order to overcome this difficulty. As an example, a function using the measured position, velocity, and torque has been derived to carry out a click-feeling knob. This function has been combined with the previous controller to create a haptic sensation. Experiments demonstrated a high quality haptic feeling.

Acknowledgment

This work was jointly supported by the National Science Foundation (DMI-9984051, CMS-0301338, CMS-0422720) and the

General Motors Corporation. Any opinions, findings, conclusions or recommendations expressed in this publication are those of the authors and do not necessarily reflect the views of the National Science Foundation.

References

[1] BMW iDrive Controller: http://www.bmwworld.com/models/e65.htm, 2002.

[2] Kuenzner, H. et al., 1999, "Operating Device for Menu Controlled Functions of a Vehicle," US005,956,016.

[3] Levin, M. et al., 2000, "Control Knob with Multiple Degrees of Freedom and Force Feedback," US006,154,201.

[4] Mannesmann VDO AG Information Systems, "Programmable Rotating Actuator with Haptic Feedback," product description, www.vdo.com.

[5] Badescu, M., Wampler, C., and Mavroidis, C., 2002, "Rotary Haptic Knob for Vehicular Instrument Controls", *Proceedings of the Tenth Symposium on Haptic Interfaces for Virtual Environment and Teleoperator Systems*, March 24, 25, 2002, Marriott Hotel, Orlando, FL.

[6] Ackermann, B., and Elferich, R., 2002, "Application of Magnetorheological Fluids in Programmable Haptic Knobs," *Actuator 2000, Seventh International Conference on New Actuators*, June 19–21, 2002, Bremen, Germany.

[7] Phule, P., and Ginder, J., 1998, "The Materials Science of Field-Responsive Fluids," MRS Bull., **23**(8), pp. 19–21.

[8] Mavroidis, C., Bar-Cohen, Y., and Bouzit, M., 2001, "Chapter 19: Haptic Interfaces Using Electrorheological Fluids," invited chapter in *Electroactive Polymer (EAP) Actuators as Artificial Muscles: Reality, Potentials and Challenges*, Y. Bar-Cohen, ed., SPIE Optical Engineering Press, Bellingham, WA, pp. 567–594.

[9] Kenaley, G. L., and Cutkosky, M. R., 1989, "Electrorheological Fluid-Based Robotic Fingers With Tactile Sensing," *Proceedings of the 1989 IEEE International Conference on Robotics and Automation*, Scottsdale, AZ, pp. 132–136.

[10] Wood, D., 1998, "Editorial: Tactile Displays: Present and Future," Displays-Technology and Applications, **18**(3), pp. 125–128.

[11] Monkman, G. J., 1992, "Electrorheological Tactile Display," *Presence*, MIT Press, Vol. 1, No. 2.

[12] Taylor, P. M., Hosseini-Sianaki, A., and Varley, C. J., 1996, "Surface Feedback for Virtual Environment Systems Using Electrorheological Fluids," Int. J. Mod. Phys. B, **10**(23–24), pp. 3011–3018.

[13] Sakaguchi, M., and Furusho, J., 1998, "Force Display System Using Particle-Type Electrorheological Fluids," *Proceedings of the 1998 IEEE International Conference on Robotics and Automation*, Leuven, Belgium, May 1998, pp. 2586–2590.

[14] Böse, H., Berkemeier, J., and Trendler, A., 2000, "Haptic System Based on Electrorheological Fluid," *Proceedings of the ACTUATOR 2000 Conference*, 19–21 June 2000, Bremen, Germany.

[15] Choi, S. B., 1999, "Control of ER Devices," Int. J. Mod. Phys. B, **13**(14–16), pp. 2160–2167.

[16] Powell, J. A., 1995, "ERF as a Means of Vibration Suppression," *Proceedings of the International Conference on Vibration and Noise*, April 25–27, 1995, pp. 1–8.

[17] Rettig, U., and Von Stryk, O., 2001, Numerical Optimal Control Strategies for Semi-Active Vehicle Suspension With ERF Dampers," in *Fast Solution of Discretized Optimization Problems*, K.-H. Hoffmann, R. H. W. Hoppe, V. Schulz, eds., ISNM Vol. 138, Birkhauser, Verlag, Basel, 2001, pp. 221–241.

[18] Gavin, H. P., 2001, "Control of Seismically-Excited Vibration Using ER Materials and Lyapunov Methods," IEEE Trans. Autom. Control, **9**(1), pp. 27–36.

[19] Nakano, M., Minagawa, S., and Hagino, K., 1999, "PMW Flow Rate Control of ER Valve and its Application to ER Actuator Control," Int. J. Mod. Phys. B, **13**(14–16), pp. 2168–2175.

[20] Akella, P., and Cutkosky, M., 1995, "Contact Transition Control with Semi-active Fingertips," IEEE Trans. Rob. Autom., **11**(6), pp. 859–867.

[21] Fisch, A., Mavroidis, C., Melli-Huber, J., and Bar-Cohen, Y., 2003, "Chapter 4: Haptic Devices for Virtual Reality, Telepresence, and Human-Assistive Robotics," invited chapter in *Biologically-Inspired Intelligent Robots*, Y. Bar-Cohen and C. Breazeal, eds., SPIE Press, Bellingham, WA, pp. 73–101.

[22] Mavroidis, C., Pfeiffer, C., Celestino, J., and Bar-Cohen, Y., 2000, "Design and Modeling of an Electro-Rheological Fluid Based Haptic Interface," *Proceedings of the 2000 ASME Mechanisms and Robotics Conference*, Baltimore, MD, September 10–13, 2000. Paper DETC2000/MECH-14121.

[23] Melli-Huber, J., Weinberg, B., Fisch, A., Nikitczuk, J., Mavroidis, C., Wampler, C., 2003, "Electro-Rheological Fluidic Actuators for Haptic Vehicular Instrument Controls," *Proceedings of the Eleventh Symposium on Haptic Interfaces for Virtual Environment and Teleoperator Systems*, March 22 and 23, 2003, Los Angeles, CA, pp. 262–267.

[24] Block, H., and Kelly, J. P., 1988, "Electro-Rheology," J. Phys. D, **21**, pp. 1661–1677.

[25] Conrad, H., 1998, "Properties and Design of Electrorheological Suspensions," MRS Bull., **23**(8), pp. 35–42.

[26] Gast, A. P., and Zukoski, C. F., 1989, "Electrorheological Suspensions as Colloidal Suspensions," Adv. Colloid Interface Sci., **30**, pp. 153–202.

[27] Weiss, K. D., Carlson, D. J., and Coulter, J. P., "Material Aspects of Electrorheological Systems," in *Advances in Intelligent Material Systems and Structures-Volume 2: Advances Electrorheological Fluids*, Kohudic, M. A., ed., Technomic Publishing Company, Lancaster, PA.

[28] Winslow, W. M., 1949, "Induced Fibrillation of Suspensions," J. Appl. Phys., **20**, pp. 1137–1140.

[29] Goodwin, J. W., Markham, G. M., and Vincent, B., 1997, "Studies on Model Electro Rheological Fluids," Adv. Organomet. Chem., **101**(11), pp. 1961–1967.

[30] Rajagopal, K. R., and Ruzicka, M., 1996, "On the Modelling of Electrorheological Materials," Mech. Res. Commun., **23**(4), pp. 401–407.

[31] Bonnecaze, R. T., and Brady, J. F., 1992, "Yield Stresses in Electrorheological Fluids," J. Rheol., **36**, 73–115.

[32] Wang, X., and Gordaninejad, F., 1999, "Flow Analysis of Field-Controllable, Electrorheological and Magnetorheological Fluids Using Herschel-Bulkley Model," J. Intell. Mater. Syst. Struct., **10**, pp. 601–608.

[33] Smart Technology Ltd, "Technical Information Sheet—Electro-Rheological Fluid LID 3354S," 2001.